

**Comparative Study of Various Control Methods for
Attitude Control of a LEO Satellite¹**

Chang-Hee Won

Satellite Communications Technology Division,

Electronics and Telecommunications Research Institute,

Yusong P.O. Box 106, Taejon, Korea 305-600

Tel: (82-42) 860-4876, Fax: (82-42) 860-6949, Email: won@etri.re.kr

Abstract

A nonlinear attitude model of a satellite with thrusters, gravity torquers and a reaction wheel cluster is developed. Then the linearized version of this satellite attitude model is derived for the attitude hold mode. For comparison purpose, various control methods are considered for attitude control of a satellite. We consider a proportional derivative controller which is actually used in the remote sensing satellite, KOMPSAT. Then a comparison is made with an H_2 controller, an H_∞ controller, and a mixed H_2/H_∞ controller. The analysis and numerical studies show that the proportional derivative controller's performance is limited in the sense that the pitch angle cannot approach zero. The simulations also show that among three control methods (H_2 control, H_∞ control, and mixed H_2/H_∞ control) H_2 control has the fastest response time, H_∞ control has the slowest and mixed H_2/H_∞ control comes in between the first two control methods. On the other hand, H_∞ control used least amount of control effort while H_2 control required the most.

Key Words: H_2/H_∞ , control, spacecraft, attitude, robust

¹ Published in *Aerospace Science and Technology*, 1999, no. 5, pp. 323-333.

1. Introduction

The desire and need to precisely control a spacecraft's attitude lead to active research in the satellite attitude control area throughout the years. Parlos and Sunkel derived the fully coupled equations of motion and linearized around an equilibrium point for a spacecraft with control moment gyro [6]. They used a full state feedback LQR (H_2) controller with gain scheduled adaptation. In the paper by Wie and *et al.*, a new approach to control the attitude of the space station has been proposed [7]. There they found the linearized equation of motion and attitude kinematics and used the LQR and pole placement techniques to control the attitude of the space station. In 1996, Ballois and Duc noted that a new LQR controller has been synthesized for one position of the solar array, and the controller change is needed for other positions. Thus they proposed an H_∞ controller to meet the performance and robustness objectives [1]. As recently as 1997, Kida *et al.* Have compared linear quadratic Gaussian control with H_∞ control for a flexible spacecraft ETS-VI [4]. Even though various control methods have been used throughout the literature, to the best of our knowledge, a comparison of the spacecraft attitude control methods using PD, H_2 control, H_∞ control, and mixed H_2/H_∞ control have not been done. The application of mixed H_2/H_∞ control to spacecraft attitude control also has not been done in the literature.

This paper develops the general nonlinear model of a low earth orbiting satellite with four thrusters, three magnetic torquers, and a four reaction wheel cluster as actuators, in the next section. In Section 3, a linearized satellite attitude model is derived for the attitude hold mode. Section 4 describes various control methods; proportional derivative (PD) control, H_2 control, H_∞ control, and mixed H_2/H_∞ control. Mixed H_2/H_∞ results are from the Nash game approach of Limebeer *et al.* [5]. In Section 5, numerical studies are performed with the real parameters of KOMPSAT, Korea Multipurpose Satellite, and the performances of the four controllers are compared. Finally, conclusions and further research directions are given in the last section.

2. Nonlinear Satellite Attitude Model

We begin the discussion by defining the local vertical local horizontal (LVLH) coordinate system. The z-axis of the LVLH coordinate system originates at the center of mass of the satellite and passes through the center of the earth. The y-axis points in the opposite direction of instantaneous orbital angular momentum vector. The direction of the x-axis is chosen to complete the right-handed coordinate system and is in the direction of the spacecraft velocity. This LVLH system does not rotate with the body of the spacecraft. The origin of body fixed coordinate (BFC) is fixed at the satellite mass center and rotates with the satellite at angular rate, $\underline{\omega}$. The z-axis of the BFC is defined as the axis of symmetry of the spacecraft primary axis, the x-axis is perpendicular to the z-axis and passes through a fixed point on the spacecraft body, and the y-axis completes the right handed triad. Consider a satellite with four thrusters, three magnetic torquers, and a four reaction wheels cluster as the actuators. Then the general nonlinear satellite attitude dynamics model can be described as

$$I_g \dot{\underline{\omega}} = -\underline{\omega} \times (I_t \underline{\omega} + L' I_w \underline{\Omega}) - L' \underline{\tau}_w + \underline{\tau}_{thruster} + \underline{\tau}_{gravity} + \underline{\tau}_{aero} + \underline{\tau}_{magnetic} + \underline{\tau}_{srp} \quad (1)$$

$$\dot{\underline{h}}_w = \underline{\tau}_w \quad (2)$$

$$\underline{h}_w = I_w \underline{\Omega} + I_w L \underline{\omega} \quad (3)$$

where

I_t : Total moment of inertia for the satellite body (3x3)

I_w : Moment of inertial matrix for the wheels (4x4)

$I_g = I_t - L' I_w L$: Total moment of inertia minus the moment of inertia of the wheels (3x3)

L : Wheel orientation matrix (4x3)

$\underline{\omega}$: Angular velocity vector in BFC (3x1)

$\underline{\Omega}$: Wheel speed vector

$\underline{\tau}_w$: Absolute torque due to the reaction wheels

$\underline{\tau}_{thruster}$: Torque due to the thrusters

$\underline{\tau}_{gravity}$: Torque due to the Earth's gravity gradient

$\underline{\tau}_{aero}$: Aerodynamic torque due to the atmospheric drag

$\underline{\tau}_{magnetic}$: Torque due to the magnetic field

$\underline{\tau}_{srp}$: Torque due to the solar radiation pressure

\underline{h}_w : Angular momentum of the wheel cluster

and the prime, ('), notation is used to denote the transposition. Figure 1 shows the configuration of four reaction wheels for a LEO satellite. The orientation matrix L is given by

$$L = \begin{bmatrix} \cos \alpha \sin \beta & \sin \alpha \sin \beta & \cos \beta \\ -\sin \alpha \sin \beta & \cos \alpha \sin \beta & \cos \beta \\ -\cos \alpha \sin \beta & -\sin \alpha \sin \beta & \cos \beta \\ \sin \alpha \sin \beta & -\cos \alpha \sin \beta & \cos \beta \end{bmatrix}. \quad (4)$$

From Equations (1), (2), and (3), we obtain the wheel dynamics equation. Take time derivative of Equation (3) and substitute it into Equation (2). Then solve for the $\underline{\dot{\Omega}}$. This gives the wheel dynamics equation:

$$\underline{\dot{\Omega}} = I_w^{-1} \underline{\tau}_w - L \underline{\dot{\omega}} \quad (5)$$

Now, substitute Equation (1) into Equation (5) to obtain,

$$\underline{\dot{\Omega}} = I_w^{-1} \underline{\tau}_w - L[-I_g^{-1} \underline{\omega} \times (I_t \underline{\omega} + L' I_w \underline{\Omega}) + I_g^{-1} (\underline{\tau}_{thruster} + \underline{\tau}_{gravity} + \underline{\tau}_{aero} + \underline{\tau}_{magnetic} + \underline{\tau}_{srp} - L' \underline{\tau}_w)] \quad (6)$$

Attitude control requires coordinate transformation from LVLH to BFC. To keep the satellite attitude Earth pointing, the satellite body axes have to be aligned with LVLH axes. Pitch (θ)-yaw (ψ)-roll (ϕ) transformation matrix can be represented using Euler angles as follows.

$$\begin{bmatrix} x \\ y \\ z \end{bmatrix}_{BFC} = \begin{bmatrix} \cos \psi \cos \theta & \sin \psi & -\cos \psi \sin \theta \\ -\cos \phi \sin \psi \cos \theta + \sin \phi \sin \theta & \cos \phi \cos \psi & \cos \phi \sin \psi \sin \theta + \sin \phi \cos \theta \\ \sin \phi \sin \psi \cos \theta + \cos \phi \sin \theta & -\sin \phi \cos \psi & -\sin \phi \sin \psi \sin \theta + \cos \phi \cos \theta \end{bmatrix} \begin{bmatrix} x_L \\ y_L \\ z_L \end{bmatrix}_{LVLH}$$

$$\equiv \begin{bmatrix} c_1 & c_2 & c_3 \end{bmatrix} \begin{bmatrix} x_L \\ y_L \\ z_L \end{bmatrix}_{LVLH}$$

(7)

On the other hand, Pitch-yaw-roll body-axes sequence attitude kinematics are represented by

$$\begin{bmatrix} \dot{\phi} \\ \dot{\theta} \\ \dot{\psi} \end{bmatrix} = \frac{1}{\cos \psi} \begin{bmatrix} \cos \psi & -\cos \phi \sin \psi & \sin \phi \sin \psi \\ 0 & \cos \phi & -\sin \phi \\ 0 & \sin \phi \cos \psi & \cos \phi \cos \psi \end{bmatrix} \begin{bmatrix} \omega_x \\ \omega_y \\ \omega_z \end{bmatrix} + \begin{bmatrix} 0 \\ n \\ 0 \end{bmatrix}, \text{ where } n \text{ is the orbital rate.}$$
(8)

Here we only consider gravity torque. Magnetic and aerodynamic torques are considered as the disturbances, and solar radiation torque is ignored. See reference [3] for details of magnetic, aerodynamic, and solar radiation torques.

The gravity gradient torque for a point mass is given by [3, p.286]

$$\begin{aligned} \underline{\tau}_{gravity} &= 3n^2 \underline{c}_3^\times I_t \underline{c}_3 \\ &= 3n^2 \begin{bmatrix} 0 & \sin \phi \sin \psi \sin \theta - \cos \phi \cos \theta & \cos \phi \sin \psi \sin \theta + \sin \phi \cos \theta \\ -\sin \phi \sin \psi \sin \theta + \cos \phi \cos \theta & 0 & \cos \psi \sin \theta \\ -\cos \phi \sin \psi \sin \theta - \sin \phi \cos \theta & -\cos \psi \sin \theta & 0 \end{bmatrix} \\ &\quad I_t \begin{bmatrix} -\cos \psi \sin \theta \\ \cos \phi \sin \psi \sin \theta + \sin \phi \cos \theta \\ -\sin \phi \sin \psi \sin \theta + \cos \phi \cos \theta \end{bmatrix} \end{aligned}$$
(9)

where n : Orbital angular rate, and \underline{c}_3^\times represents the cross product matrix of a vector \underline{c}_3 defined in Equation (7).

3. Linear Satellite Attitude Model

Here we consider controlling the satellite's attitude using a cluster of reaction wheels and thrusters. For the LEO satellites with the altitude from 400km to 2500km, the largest torque is the gravitational torque. See [3, p.271]. Thus we incorporate the gravitational torque into the system equation. The second and third largest torques affecting the satellites are the aerodynamic torque and the magnetic torque. Thus we consider these torques as the external disturbances. The solar radiation pressure (diffuse reflection and specular reflections), the effects due to solar and lunar

gravitation, and charged particles are ignored because they are much smaller than the gravitational, magnetic and aerodynamic torques [3, p.271]. Thus Equation (1) becomes

$$I_g \dot{\underline{\omega}} = -\underline{\omega} \times (I_t \underline{\omega} + L' I_w \underline{\Omega}) - L' \underline{\tau}_w + \underline{\tau}_{thruster} + 3n^2 \underline{c}_3 \times I_t \underline{c}_3 + \underline{w} \quad (10)$$

where $\underline{w} = \underline{\tau}_{aero} + \underline{\tau}_{magnetic}$

If we assume small attitude variations from LVLH coordinates, the above equation can be linearized in the state space form around a certain equilibrium point as follows:

$$\dot{\underline{x}} = \left(\frac{\partial f}{\partial \underline{x}'} \right) \underline{x} + \left(\frac{\partial f}{\partial \underline{u}'} \right) \underline{u} + \left(\frac{\partial f}{\partial \underline{w}'} \right) \underline{w} \quad (11)$$

$$\dot{\underline{x}} = A \underline{x} + B \underline{u} + E \underline{w} \quad (12)$$

where $\underline{x} = [\phi, \theta, \psi, \omega_x, \delta\omega_y, \omega_z, \Omega_1, \Omega_2, \Omega_3, \Omega_4]'$ and $\underline{u} = [\tau_w \ \tau_{thruster}]'$

To have zero initial conditions we let $\delta\omega_y = \omega_y + n$, and find the general linear equation for any torque equilibrium attitude (TEA) of the states. For the simplicity sake, here we assume the case of the attitude hold mode where the TEA values are fixed at the following values:

$\underline{x}_0 = [0,0,0,0,0,0,0,0,0,0]'$. Then the following matrices can be defined

$$I_t = \begin{bmatrix} I_t(1,1) & I_t(1,2) & I_t(1,3) \\ I_t(2,1) & I_t(2,2) & I_t(2,3) \\ I_t(3,1) & I_t(3,2) & I_t(3,3) \end{bmatrix} \quad I_w = \begin{bmatrix} I_w(1,1) & 0 & 0 & 0 \\ 0 & I_w(2,2) & 0 & 0 \\ 0 & 0 & I_w(3,3) & 0 \\ 0 & 0 & 0 & I_w(4,4) \end{bmatrix}$$

$$L = \begin{bmatrix} L(1,1) & L(1,2) & L(1,3) \\ L(2,1) & L(2,2) & L(2,3) \\ L(3,1) & L(3,2) & L(3,3) \\ L(4,1) & L(4,2) & L(4,3) \end{bmatrix} \quad L' = \begin{bmatrix} L_t(1,1) & L_t(1,2) & L_t(1,3) & L_t(1,4) \\ L_t(2,1) & L_t(2,2) & L_t(2,3) & L_t(2,4) \\ L_t(3,1) & L_t(3,2) & L_t(3,3) & L_t(3,4) \end{bmatrix}$$

$$I_g^{-1} = \begin{bmatrix} I_{ginv}(1,1) & I_{ginv}(1,2) & I_{ginv}(1,3) \\ I_{ginv}(2,1) & I_{ginv}(2,2) & I_{ginv}(2,3) \\ I_{ginv}(3,1) & I_{ginv}(3,2) & I_{ginv}(3,3) \end{bmatrix} \quad \underline{\tau}_w = \begin{bmatrix} \tau_{w1} \\ \tau_{w2} \\ \tau_{w3} \\ \tau_{w4} \end{bmatrix} \quad (13)$$

Now we expand the first term on the right hand side of Equation (10),

$$\begin{aligned}
-\underline{\omega} \times I_t \underline{\omega} &= \begin{bmatrix} 0 & \omega_z & -(\delta\omega_y - n) \\ -\omega_z & 0 & \omega_x \\ \delta\omega_y - n & -\omega_x & 0 \end{bmatrix} \begin{bmatrix} It(1,1) & It(1,2) & It(1,3) \\ It(2,1) & It(2,2) & It(2,3) \\ It(3,1) & It(3,2) & It(3,3) \end{bmatrix} \begin{bmatrix} \omega_x \\ \delta\omega_y - n \\ \omega_z \end{bmatrix} \\
&= \begin{bmatrix} It(2,1)\omega_z\omega_x - It(3,1)\omega_x(\delta\omega_y - n) + It(2,2)\omega_z(\delta\omega_y - n) - It(3,2)(\delta\omega_y - n)^2 + It(2,3)\omega_z^2 - It(3,3)(\delta\omega_y - n)\omega_z \\ -It(1,1)\omega_z\omega_x + It(3,1)\omega_x^2 - It(1,2)\omega_z(\delta\omega_y - n) + It(3,2)(\delta\omega_y - n)\omega_x - It(1,3)\omega_z^2 + It(3,3)\omega_z\omega_x \\ It(1,1)(\delta\omega_y - n)\omega_x - It(2,1)\omega_x^2 + It(1,2)(\delta\omega_y - n)^2 - It(2,2)(\delta\omega_y - n)\omega_x + It(1,3)(\delta\omega_y - n)\omega_z - It(2,3)\omega_z\omega_x \end{bmatrix} \quad (14)
\end{aligned}$$

then linearize around the TEA to obtain,

$$\begin{bmatrix} It(3,1)n & 2It(3,2)n & It(2,2)(-n) + It(3,3)n \\ -nIt(3,2) & 0 & It(1,2)n \\ n(It(2,2) - It(1,1)) & -2nIt(1,2) & -It(1,3)n \end{bmatrix} \begin{bmatrix} \omega_x \\ \delta\omega_y \\ \omega_z \end{bmatrix}. \quad (15)$$

Then the second term on the right hand side of Equation (10) is expanded as follows:

$$\begin{aligned}
-\underline{\omega} \times L' I_w \underline{\Omega} &= \begin{bmatrix} 0 & \omega_z & -(\delta\omega_y - n) \\ -\omega_z & 0 & \omega_x \\ \delta\omega_y - n & -\omega_x & 0 \end{bmatrix} \begin{bmatrix} Lt(1,1) & Lt(1,2) & Lt(1,3) & Lt(1,4) \\ Lt(2,1) & Lt(2,2) & Lt(2,3) & Lt(2,4) \\ Lt(3,1) & Lt(3,2) & Lt(3,3) & Lt(3,4) \end{bmatrix} \\
&\quad \begin{bmatrix} Iw(1,1) & 0 & 0 & 0 \\ 0 & Iw(2,2) & 0 & 0 \\ 0 & 0 & Iw(3,3) & 0 \\ 0 & 0 & 0 & Iw(4,4) \end{bmatrix} \begin{bmatrix} \Omega_1 \\ \Omega_2 \\ \Omega_3 \\ \Omega_4 \end{bmatrix} \\
&= \begin{bmatrix} Iw(1,1)\Omega_1\omega_z Lt(2,1) + Iw(2,2)\Omega_2\omega_z Lt(2,2) + Iw(3,3)\Omega_3\omega_z Lt(2,3) + Iw(4,4)\Omega_4\omega_z Lt(2,4) - Iw(1,1)\Omega_1(\delta\omega_y - n)Lt(3,1) \\ -Iw(2,2)\Omega_2(\delta\omega_y - n)Lt(3,2) - Iw(3,3)\Omega_3(\delta\omega_y - n)Lt(3,3) - Iw(4,4)\Omega_4(\delta\omega_y - n)Lt(3,4) \\ -Iw(1,1)\Omega_1\omega_z Lt(1,1) - Iw(2,2)\Omega_2\omega_z Lt(1,2) - Iw(3,3)\Omega_3\omega_z Lt(1,3) - Iw(4,4)\Omega_4\omega_z Lt(1,4) + Iw(1,1)\Omega_1\omega_x Lt(3,1) \\ + Iw(2,2)\Omega_2\omega_x Lt(3,2) + Iw(3,3)\Omega_3\omega_x Lt(3,3) + Iw(4,4)\Omega_4\omega_x Lt(3,4) \\ Iw(1,1)\Omega_1(\delta\omega_y - n)Lt(1,1) + Iw(2,2)\Omega_2(\delta\omega_y - n)Lt(1,2) + Iw(3,3)\Omega_3(\delta\omega_y - n)Lt(1,3) + Iw(4,4)\Omega_4(\delta\omega_y - n)Lt(1,4) \\ -Iw(1,1)\Omega_1\omega_x Lt(2,1) - Iw(2,2)\Omega_2\omega_x Lt(2,2) - Iw(3,3)\Omega_3\omega_x Lt(2,3) - Iw(4,4)\Omega_4\omega_x Lt(2,4) \end{bmatrix} \quad (16)
\end{aligned}$$

These equations are linearized around TEA to obtain

$$n \begin{bmatrix} Iw(1,1)Lt(3,1) & Iw(2,2)Lt(3,2) & Iw(3,3)Lt(3,3) & Iw(4,4)Lt(3,4) \\ 0 & 0 & 0 & 0 \\ -Iw(1,1)Lt(1,1) & -Iw(2,2)Lt(1,2) & -Iw(3,3)Lt(1,3) & -Iw(4,4)Lt(1,4) \end{bmatrix} \begin{bmatrix} \Omega_1 \\ \Omega_2 \\ \Omega_3 \\ \Omega_4 \end{bmatrix}. \quad (17)$$

Linearizing other terms in a similar manner, we obtain the following linear equations from Equation (10).

$$\begin{aligned}
I_g \underline{\dot{\omega}} = & n \begin{bmatrix} It(3,1) & 2It(3,2) & It(3,3) - It(2,2) \\ -It(3,2) & 0 & It(1,2) \\ It(2,2) - It(1,1) & -2It(1,2) & -It(1,3) \end{bmatrix} \begin{bmatrix} \omega_x \\ \delta\omega_y \\ \omega_z \end{bmatrix} \\
& + n \begin{bmatrix} Iw(1,1)Lt(3,1) & Iw(2,2)Lt(3,2) & Iw(3,3)Lt(3,3) & Iw(4,4)Lt(3,4) \\ 0 & 0 & 0 & 0 \\ -Iw(1,1)Lt(1,1) & -Iw(2,2)Lt(1,2) & -Iw(3,3)Lt(1,3) & -Iw(4,4)Lt(1,4) \end{bmatrix} \begin{bmatrix} \Omega_1 \\ \Omega_2 \\ \Omega_3 \\ \Omega_4 \end{bmatrix} \\
& + 3n^2 \begin{bmatrix} It(3,3) - It(2,2) & It(2,1) & 0 \\ It(2,1) & It(3,3) - It(1,1) & 0 \\ -It(1,3) & -It(2,3) & 0 \end{bmatrix} \begin{bmatrix} \phi \\ \theta \\ \psi \end{bmatrix} + n^2 \begin{bmatrix} -2It(2,3) \\ 3It(1,3) \\ -It(1,2) \end{bmatrix} - L' \underline{\tau}_w + \underline{\tau}_{thruster} + \underline{w}
\end{aligned} \tag{18}$$

Assuming that the products of inertia of the satellite body are small, we obtain

$$\begin{aligned}
\underline{\dot{\omega}} = & I_g^{-1} n \begin{bmatrix} 0 & 0 & It(3,3) - It(2,2) \\ 0 & 0 & 0 \\ It(2,2) - It(1,1) & 0 & 0 \end{bmatrix} \begin{bmatrix} \omega_x \\ \delta\omega_y \\ \omega_z \end{bmatrix} \\
& + I_g^{-1} n \begin{bmatrix} Iw(1,1)Lt(3,1) & Iw(2,2)Lt(3,2) & Iw(3,3)Lt(3,3) & Iw(4,4)Lt(3,4) \\ 0 & 0 & 0 & 0 \\ -Iw(1,1)Lt(1,1) & -Iw(2,2)Lt(1,2) & -Iw(3,3)Lt(1,3) & -Iw(4,4)Lt(1,4) \end{bmatrix} \begin{bmatrix} \Omega_1 \\ \Omega_2 \\ \Omega_3 \\ \Omega_4 \end{bmatrix}, \\
& + I_g^{-1} 3n^2 \begin{bmatrix} It(3,3) - It(2,2) & 0 & 0 \\ 0 & It(3,3) - It(1,1) & 0 \\ 0 & 0 & 0 \end{bmatrix} \begin{bmatrix} \phi \\ \theta \\ \psi \end{bmatrix} - I_g^{-1} L' \underline{\tau}_w + I_g^{-1} \underline{\tau}_{thruster} + I_g^{-1} \underline{w}
\end{aligned} \tag{19}$$

$$\underline{\dot{\omega}} \equiv I_g^{-1} n N_1 \begin{bmatrix} \omega_x \\ \delta\omega_y \\ \omega_z \end{bmatrix} + I_g^{-1} n N_2 \begin{bmatrix} \Omega_1 \\ \Omega_2 \\ \Omega_3 \\ \Omega_4 \end{bmatrix} + I_g^{-1} 3n^2 N_3 \begin{bmatrix} \phi \\ \theta \\ \psi \end{bmatrix} - I_g^{-1} L' \underline{\tau}_w + I_g^{-1} \underline{\tau}_{thruster} + I_g^{-1} \underline{w}. \tag{19}$$

Assuming that (ϕ, θ, ψ) are small in magnitude, the attitude kinematics, expressed by Equation (8),

can be linearized around TEA to obtain,

$$\begin{bmatrix} \dot{\phi} \\ \dot{\theta} \\ \dot{\psi} \end{bmatrix} = \begin{bmatrix} 0 \\ 0 \\ -n \end{bmatrix} \phi + \begin{bmatrix} n \\ 0 \\ 0 \end{bmatrix} \psi + \begin{bmatrix} 1 \\ 0 \\ 0 \end{bmatrix} \omega_x + \begin{bmatrix} 0 \\ 1 \\ 0 \end{bmatrix} (\omega_y + n) + \begin{bmatrix} 0 \\ 0 \\ 1 \end{bmatrix} \omega_z \tag{20}$$

Because $\delta\omega_y = \omega_y + n$, we have

$$\begin{aligned}
\dot{\phi} &= n\psi + \omega_x \\
\dot{\theta} &= \omega_y + n = \delta\omega_y \\
\dot{\psi} &= -n\phi + \omega_z
\end{aligned} \tag{21}$$

Also the wheel dynamics equation given in Equation (5) is

$$\dot{\underline{\Omega}} = I_w^{-1} \underline{\tau}_w - L \underline{\dot{\omega}}. \tag{22}$$

Using Equations (19), (21), and (22), a linear differential equation is formed:

$$\frac{d}{dt} \begin{bmatrix} \phi \\ \theta \\ \psi \\ \omega_x \\ \delta\omega_y \\ \omega_z \\ \Omega_1 \\ \Omega_2 \\ \Omega_3 \\ \Omega_4 \end{bmatrix} = A \begin{bmatrix} \phi \\ \theta \\ \psi \\ \omega_x \\ \delta\omega_y \\ \omega_z \\ \Omega_1 \\ \Omega_2 \\ \Omega_3 \\ \Omega_4 \end{bmatrix} + B \begin{bmatrix} \underline{\tau}_w \\ \underline{\tau}_{thruster} \end{bmatrix} + E \underline{w} \tag{23}$$

where

$$A = \begin{bmatrix} 0 & 0 & n & 1 & 0 & 0 & & & & & \\ 0 & 0 & 0 & 0 & 1 & 0 & & & & & 0_{3 \times 4} \\ -n & 0 & 0 & 0 & 0 & 1 & & & & & \\ 3I_g^{-1}n^2N_3 & I_g^{-1}nN_1 & I_g^{-1}nN_2 & & & & & & & & \\ -L3I_g^{-1}n^2N_3 & -LI_g^{-1}nN_1 & -LI_g^{-1}nN_2 & & & & & & & & \end{bmatrix} \quad B = \begin{bmatrix} 0_{3 \times 4} & 0_{3 \times 3} \\ -I_g^{-1}L' & I_g^{-1} \\ I_w^{-1} + LI_g^{-1}L' & -LI_g^{-1} \end{bmatrix}$$

$$E = \begin{bmatrix} 0_{3 \times 3} & 0_{3 \times 3} & 0_{3 \times 3} \\ I_g^{-1} & I_g^{-1} & I_g^{-1} \\ -LI_g^{-1} & -LI_g^{-1} & -LI_g^{-1} \end{bmatrix} \quad \text{and } N_1, N_2, \text{ and } N_3 \text{ are defined in Equation (19).}$$

Note that roll, pitch, and yaw are coupled even though the products of inertia of the spacecraft are small. This is because more general satellite attitude dynamics model, see Equation (1), with the reaction wheels is used in the derivation.

4. Control Methods

PD Control:

The Proportional Derivative (PD) Control law for the system given by Equation (10) is

$$L' \underline{u} = -\underline{\omega} \times (I_t \underline{\omega} + L' I_w \underline{\Omega}) + D \underline{\omega} + K \underline{\phi}_e \quad (24)$$

where $\underline{\omega} = [\omega_x, \omega_y, \omega_z]'$, $\underline{\phi}_e = [\phi, \theta, \psi]'$, $D = d[I_t - L' I_w L]$, and $K = k[I_t - L' I_w L]$.

Then Equation (10) becomes

$$\dot{\underline{\omega}} = -d \underline{\omega} - k \underline{\phi}_e + I_g^{-1} 3n^2 \underline{c}_3^x I_t \underline{c}_3 + I_g^{-1} \underline{w}. \quad (25)$$

The gravity term, $I_g^{-1} 3n^2 \underline{c}_3^x I_t \underline{c}_3$, is small compared to the $\underline{\omega}$ or the $\underline{\phi}_e$ terms if we assume small angle change. Also if we assume small external disturbances, we obtain

$$\dot{\underline{\omega}} = -d \underline{\omega} - k \underline{\phi}_e. \quad (26)$$

This is a simple first order system with the dc gain $-\frac{k}{d}$ and the time constant $\frac{1}{d}$. The dc gain establishes the final value the output approaches, and the time constant information concerns the speed of the response. An advantage of a PD controller is in simplicity. It is relatively robust for a single input single output system when the plant is not accurately modeled. This approach is used in the attitude hold mode of our KOMPSAT application.

H_2 Optimal linear quadratic control:

The system state equation is defined by the following equations:

$$\dot{\underline{x}}(t) = A(t)\underline{x}(t) + B(t)\underline{u}(t), \quad x(0) = x_0 \quad (27)$$

$$\underline{z}(t) = \begin{bmatrix} C(t)\underline{x}(t) \\ D(t)\underline{u}(t) \end{bmatrix} \quad D'(t)D(t) = I \quad (28)$$

Note that $C' C = Q$ and $D' D = R$ are the weighting matrices. The cost function is given by

$$J_2 = \min_u \left\{ \int_0^T \underline{z}'(t)\underline{z}(t) dt \right\} \quad (29)$$

The solution is well known for the full-state-feedback linear quadratic optimal control problem. See [2, p.408] for example. The optimal control is given by

$$\underline{u}^*(t, x) = -B'(t)P(t)\underline{x}(t), \quad (30)$$

where P is given by the following Riccati equation [2, p.408]:

$$-P(t) = A'(t)P(t) + P(t)A(t) - P(t)B(t)B'(t)P(t) + C'C, \quad P(T) = 0. \quad (31)$$

The cost function given by Equation (29) is quadratic in both states and control variables. It represents the energy of the system. Thus, H_2 control can be interpreted as energy minimization. The advantage of this method is that there exist extensive theory associated with this method, and good performance (at least 6dB gain margin and 60 degrees phase margin) is guaranteed according to those theories [8, p. 383].

H_∞ Optimal control:

The system equation is given by

$$\dot{\underline{x}}(t) = A(t)\underline{x}(t) + B(t)\underline{u}(t) + E(t)\underline{w}(t), \quad \underline{x}(0) = \underline{x}_0 \quad (32)$$

$$\underline{z}(t) = \begin{bmatrix} C(t)\underline{x}(t) \\ D(t)\underline{u}(t) \end{bmatrix} \quad D'(t)D(t) = I. \quad (33)$$

The cost function is given by

$$J_1 = \int_0^T [\gamma^2 \underline{w}'(t)\underline{w}(t) - \underline{z}'(t)\underline{z}(t)] dt \quad (34)$$

which is an H_∞ criterion [5]. The optimal control is given by the following equations:

$$\underline{u}^*(t, x) = -B'(t)P_\infty(t)\underline{x}(t), \quad (35)$$

$$\underline{w}^*(t, x) = \gamma^{-2} E'(t)P_\infty(t)\underline{x}(t), \quad (36)$$

where the $P_\infty(t)$ is given by the following Riccati equation [5]:

$$-P_\infty(t) = A'(t)P_\infty(t) + P_\infty(t)A(t) - P_\infty(t)[B(t)B'(t) - \gamma^{-2}EE']P_\infty(t) + C'C, \quad P_\infty(T) = 0. \quad (37)$$

The H_∞ controller minimizes the H_∞ norm of the closed loop transfer function from the external disturbance to the error signal. The H_∞ norm gives the maximum energy gain or sinusoidal gain of the system [8, p.3]. Thus the control, \underline{u} , regulates the state, \underline{x} , in such a way as to minimize the output energy when the worst case disturbance, \underline{w} , is applied to the system. The disturbance, \underline{w} , is worst case in the sense that it achieves the maximum possible energy given from the disturbance input to the output.

Here robust stability is guaranteed, but robustness due to the parameter errors should be considered carefully.

Mixed H_2/H_∞ Optimal Control:

Mixed H_2/H_∞ control problem is solved using Nash game approach. Two-player, nonzero sum Nash differential games have two performance criteria. The idea of Limebeer *et al.* [5] is to use one performance criterion to reflect H_∞ cost and the other to reflect the H_2 cost.

$$\dot{\underline{x}}(t) = A(t)\underline{x} + B(t)\underline{u} + E(t)\underline{w}, \quad \underline{x}(0) = \underline{x}_0 \quad (38)$$

$$\underline{z}(t) = \begin{bmatrix} C(t)\underline{x}(t) \\ D(t)\underline{u}(t) \end{bmatrix} \quad D'(t)D(t) = I \quad (39)$$

The first cost function associated with the H_∞ cost is given by

$$J_1 = \int_0^T [\gamma^2 \underline{w}'(t)\underline{w}(t) - \underline{z}'(t)\underline{z}(t)] dt, \quad (40)$$

and the second cost function which is associated with the H_2 cost is given by

$$J_2 = \int_0^T [\underline{z}'(t)\underline{z}(t)] dt. \quad (41)$$

Then the problem is to find the Nash equilibrium strategies $\underline{u}^*(t, x)$ and $\underline{w}^*(t, x)$ in the set of linear memoryless feedback laws, which satisfy the following two inequalities:

$$\begin{aligned} J_1(\underline{u}^*, \underline{w}^*) &\leq J_1(\underline{u}^*, \underline{w}) \\ J_2(\underline{u}^*, \underline{w}^*) &\leq J_2(\underline{u}, \underline{w}^*) \end{aligned} \quad (42)$$

Then the solution is found to be

$$\underline{u}^*(t, x) = -B'(t)P_2(t)\underline{x}(t), \quad (43)$$

$$\underline{w}^*(t, x) = -\gamma^{-2}E'(t)P_1(t)\underline{x}(t), \quad (44)$$

where P_1 and P_2 is found from the following coupled Riccati type differential equations [5]:

$$\begin{aligned} -\dot{P}_1(t) &= A'(t)P_1(t) + P_1(t)A(t) - P_1(t)\gamma^{-2}EE'P_1(t) - P_2BB'P_1 - P_1BB'P_2 - P_2BB'P_2 - C'C, \\ -\dot{P}_2(t) &= A'(t)P_2(t) + P_2(t)A(t) - P_1(t)\rho^2\gamma^{-4}EE'P_1(t) - \gamma^{-2}P_2EE'P_1 - \gamma^{-2}P_1EE'P_2 - P_2BB'P_2 + C'C, \end{aligned} \quad (45)$$

with the boundary conditions, $P_1(T) = 0$ and $P_2(T) = 0$.

In mixed H_2/H_∞ optimal control, two cost functions are considered and the optimal controllers are found to minimize these two cost functions. Thus, this optimal control method balances between no additive external disturbance H_2 control and the worst case additive disturbance H_∞ control.

5. Simulation Results

This section contains various numerical simulations for the controllers described in the previous section, The actual parameters of low earth orbiting remote sensing satellite, KOMPSAT, has been used. The KOMPSAT is a sun-synchronous remote sensing satellite with the inclination of 98.13 degrees, the altitude of 685km, and the total weight of 509kg. It is scheduled to be launched in October of 1999. The sensors and actuators in the KOMPSAT are described in Table I.

We shall assume that roll, pitch, and yaw angles are available using the conical earth sensor, the fine sun sensor, and the gyros. Furthermore the wheel speeds are also available from the measurement of the reaction wheel tachometer.

5.1 PD Controller

On KOMPSAT, a PD controller is used for the attitude hold mode. In this numerical study, we shall show the transient response of the PD controller and compare it with the H_2 , H_∞ , and

mixed H_2 / H_∞ controller responses. The simulation parameters are orbital rate, $n = 0.0010636$ rad/s, total moment of inertia for the spacecraft body,

$$I_t = \begin{bmatrix} 294.62 & 0 & 0 \\ 0 & 129.56 & 0 \\ 0 & 0 & 209.76 \end{bmatrix} \text{ kg m}^2, \text{ moment of inertia matrix for the reaction wheels,}$$

$$I_w = 0.01044 \begin{bmatrix} 1 & 0 & 0 & 0 \\ 0 & 1 & 0 & 0 \\ 0 & 0 & 1 & 0 \\ 0 & 0 & 0 & 1 \end{bmatrix} \text{ kg m}^2, \text{ the parameters for the wheel orientation matrix, } L \text{ are given as}$$

$$\alpha = 45^\circ, \beta = 54.74^\circ, \text{ and the initial values are chosen as } [0 \quad -n \quad 0 \quad 1 \quad 1 \quad 1].$$

In Figure 2, the angular velocities of the spacecraft are plotted with respect to time for a PD controller. Here we let the PD control gain as $d=0.1$ and $k=0.01$ in Equation (26). The ω_x has an undershoot and an overshoot before settling down to zero. The response of ω_z closely resemble the response of ω_x . The ω_y has smaller variation then the other angular velocities but it settles down to the orbital rate, $-n$, instead of zero. Figure 3 shows the Euler angle responses, where θ is pitch, ψ is yaw, and ϕ is roll angles. From the initial value of 1 degree, ψ and ϕ settle down zero, while θ settles down to $10n$. This result is expected because we know that in steady state, ω_x and ω_z goes to zero and ω_y goes to $-n$ from Figure 2. Thus in steady state $\dot{\omega} = 0$ and $\underline{\omega} = [0 \quad -n \quad 0]'$, thus substitute these values into Equation (26), then we obtain $\theta \rightarrow \frac{d}{k}n$ in steady state. To make θ approach zero we have to let $d \ll k$, but then we note that the settling time increases. This is because the dc gain is $-\frac{k}{d}$ and the final value approaches zero only when this gain approaches zero. That only happens when either d is equal to zero or when d is equal to infinity. Also when the dc gain approaches zero the time constant, $\frac{1}{d}$, approaches zero, thus the speed of the response increases. Consequently, we note that it is difficult to let the pitch angle approach zero using a PD controller.

Note also that the beauty of a PD controller is in its simplicity and it is known to be very

robust when the system is not accurately modelled. For the stability analysis, we consider the maximum real part of the closed loop poles, and for this PD controller we find that the maximum real part of the closed loop pole is -0.1 .

5.2 Comparison of H_2 , H_∞ , and mixed H_2/H_∞ controllers

Figure 4 shows the angular velocity versus time graph for H_2 , H_∞ , and mixed H_2/H_∞ control methods. We use the same simulation parameters as the PD control case. The first subplot in Figure 4 shows the angular velocities $\omega_x, \omega_y, \omega_z$ versus time using an H_2 controller. The second subplot of Figure 4 is for the H_∞ controller, and the last subplot in Figure 4 is for the mixed H_2/H_∞ controller. The first subplot (H_2) shows more oscillation and slower settling time than the curves in the second subplot (H_∞). The last subplot in Figure 4 (mixed H_2/H_∞) response is close to H_2 response. For the comparison purpose, the following Table II shows that the angular velocity and time when the angular velocity ω_x is -0.002 deg/sec. Thus H_2 control gives the best performance, H_∞ control gives the worst performance, and mixed H_2/H_∞ control gives the performance in between those two control methods.

Figure 5 shows the Euler angles versus time graph. Again, the first subplot in Figure 5 is for H_2 control, the second subplot is for H_∞ control, and the third subplot is for mixed H_2/H_∞ control. Each subplot shows three curves for θ is pitch, ψ is yaw, and ϕ is roll angles. All plots show relatively good performance characteristics compared with PD control shown in Figure 3. In PD control, one of the Euler angles, θ , does not approach zero. Thus all three controllers perform better than PD controller. Although it is not shown clearly in the first plot of Figure 5, there exists some undershoot for the H_2 controller, but not for the H_∞ controller. The Euler angles of due to the H_∞ controller decreases monotonically toward zero. Table III shows the times when the roll angle reaches 0.03 degree. Once again the H_2 control gives the fastest time.

Figure 6 shows the control action from the reaction wheels, and Figure 7 shows the control action due to the thrusters. We note that the initial action of an H_∞ controller is larger at the start but the overshoot is smaller. Also it settles down to zero faster than the H_2 controller. Once again, the control action of mixed H_2/H_∞ control falls in between the H_2 control and the H_∞ control. Note that the control action due to the reaction wheels are about 3 to 4 orders of magnitude smaller than the control action due to the thrusters. Table IV shows the control action required due to the reaction wheels and the thrusters for the specific times. The times are chosen to match the times of Table III. Note that H_2 control requires the largest control effort and H_∞ control requires the smallest control effort. Also note that control due to the reaction wheels are zero at those times, implying that the reaction wheels are not being used.

Finally, we show the stability results. Table V shows the maximum real part of the closed loop system poles for all four control methods. The PD control has the largest closed loop eigenvalue and H_∞ control has the smallest eigenvalue, but the differences in eigenvalues between H_2 control, H_∞ control, and mixed H_2/H_∞ control are not significant. Thus from the stability point of view all three, H_2 control, H_∞ control, and mixed H_2/H_∞ control, methods give similar stability margins.

5.3 Stability of H_2 , H_∞ , and mixed H_2/H_∞ controllers

Here we consider a time invariant system and compare the stability characteristics of H_2 , H_∞ , and mixed H_2/H_∞ controllers. For the system given in Equations (27) and (28) with an H_2 controller, the sufficient and necessary conditions for a stable closed loop optimal system with finite performance index are (A,C) detectable and (A,B) stabilizable. For an H_∞ controller, similar conditions exist which are (A,C) detectable and (A,E) stabilizable [8,p.302]. Furthermore, Limebeer showed that the conditions, (A,C) detectable and (A,E) stabilizable, guarantee the existence of optimal mixed H_2/H_∞ controller [5]. Thus it is important to check the detectability and stabilizability of the system under consideration. The system considered in the

previous section is detectable and stabilizable.

We may determine the stability characteristics of a system from the closed loop system matrix A_{cl} . From Section 4 we have

$$\begin{aligned}
 H_2 : \quad A_{cl} &= A - BB'P \\
 H_\infty : \quad A_{cl} &= A + \gamma^{-2}EE'P_\infty - BB'P_\infty \\
 \text{Mixed } H_2 / H_\infty : \quad A_{cl} &= A - \gamma^{-2}EE'P_1 - BB'P_2
 \end{aligned} \tag{46}$$

For simplicity, we consider the scalar case. Then we note that mixed H_2/H_∞ closed loop system matrix is the smallest and H_∞ closed loop system matrix is the largest. Thus, if we consider the stability margin in terms of the maximum real part of the closed loop poles, it is most likely that the mixed H_2/H_∞ controller would have the largest stability margin and H_∞ controller the smallest stability margin. In Section 5.2 Table V, we note that the above claim is verified in this particular case.

6. Conclusions

This paper presented the beginning of the study of various control methods that can be used in satellite attitude control. The control method presented in this paper are not new algorithms, however, the application of mixed H_2/H_∞ control to the satellite attitude control problem has been done for the first time. Also the comparison of four different control strategies have been performed. By comparing these performance, we expect to learn more about the differences in various control methods with possibility of applying them in the future KOMPSAT missions. The transient responses of a linear satellite attitude model are studied for four different control methods. We conclude that the PD controller is limited in the sense that it cannot achieve certain angle requirements. An H_2 controller gave the best performance and the H_∞ controller gave the worst performance out of these three control methods, and the mixed H_2/H_∞ controller gave the performance which was in between the H_2 and H_∞ controllers. The study of these controllers' characteristics with respect to the parameter uncertainties is left as the future research topic. The

next step after that study is in the direction of creating a nonlinear satellite attitude model and performing simulations using the linear controllers developed here. Then comes the step of comparing newly developed linear controllers with the more general nonlinear controllers.

7. References

- [1] S. L. Ballois and G. Duc, “ H_∞ Control of an Earth Observation Satellite,” *Journal of Guidance, Control, and Dynamics*, Vol. 19, No. 3, May-June 1996, pp. 628–635.
- [2] Bryson A.E. and Y.C. Ho, *Applied Optimal Control, Optimization, Estimation, and Control*, Revised Printing, A Halsted Press Book, John Wiley & Sons, 1975.
- [3] Hughes, P. C., *Spacecraft Attitude Dynamics*, John Wiley & Sons, New York, 1986.
- [4] Kida, T., I. Yamaguchi, Y. Chida, and T. Sekiguchi, “On-Orbit Robust Control Experiment of Flexible Spacecraft ETS-VI,” *Journal of Guidance, Control, and Dynamics*, Vol. 20, No. 5, September-October 1997, pp. 865—872.
- [5] Limebeer, D.J.N., B.D.O. Anderson, and B. Hendel, “A Nash Game Approach to Mixed H_2/H -infinity Control,” *IEEE Transactions on Automatic Control*, Vol. 39, No. 1, January 1994, pp. 69—82.
- [6] Parlos, A. G. and Sunkel J. W., “Adaptive Attitude Control and Momentum Management for Large-Angle Spacecraft Maneuvers,” *Journal of Guidance, Control, and Dynamics*, Vol. 15, No. 4, July-August 1992, pp. 1018—1028.
- [7] B. Wie, K. W. Byun, V. W. Warren, D. Geller, D. Long, and J. Sunkel, “New Approach to Attitude/Momentum Control for the Space Station,” *Journal of Guidance, Control, and Dynamics*, Vol. 12, No. 5, September-October 1989, pp. 714--722.
- [8] Zhou, K. with J. Doyle, and Keith Glover, *Robust and Optimal Control*, Prentice Hall, 1996.

Table I: Numbers of Sensors and Actuators in KOMPSAT

	Name	Number
Sensors	Gyro reference assembly	3
	GPS receiver	2
	Conical earth sensor	2
	Fine sun sensor assembly	2
	Coarse sun sensor assembly	4
	Three axis magnetometer	2
	Reaction wheel tachometer	4
	Solar array drive potentiometer	2
Actuators	Reaction wheels	4
	Thrusters	4
	Magnetic torque rods	3
	Solar array drive assemblies	2

Table II: Angular Velocity and Time of Three Control Methods

Control Method	ω_x (deg/sec)	Time (sec)
H_2 control	-0.002	58.26
H_∞ control	-0.002	82.28
mixed H_2/H_∞ control	-0.002	66.92

Table III: Roll angle and Time for Three Control Methods

Control Method	Roll angle (deg)	Time (sec)
H_2 control	0.03	45.37
H_∞ control	0.03	99.16
mixed H_2/H_∞ control	0.03	62.18

Table IV: Control Action Required for Three Control Methods

Control Method	Time (sec)	Control due to Reaction				Control due to thruster		
		Wheels				x	y	z
		W1	W2	W3	W4			
H_2 control	45.38	0.0	0.0	0.0	0.0	.0028	.0006	.0017
H_∞ control	99.16	0.0	0.0	0.0	0.0	.0001	.0000	.0000
mixed H_2/H_∞ control	62.18	0.0	0.0	0.0	0.0	.0012	.0001	.0005

Table V: Robust Stability Comparison

Control Methods	Maximum real part of the closed loop poles
PD	-0.1
H_2 control	-4.805e-2
H_∞ control	-3.399e-2
mixed H_2/H_∞ control	-6.561e-2

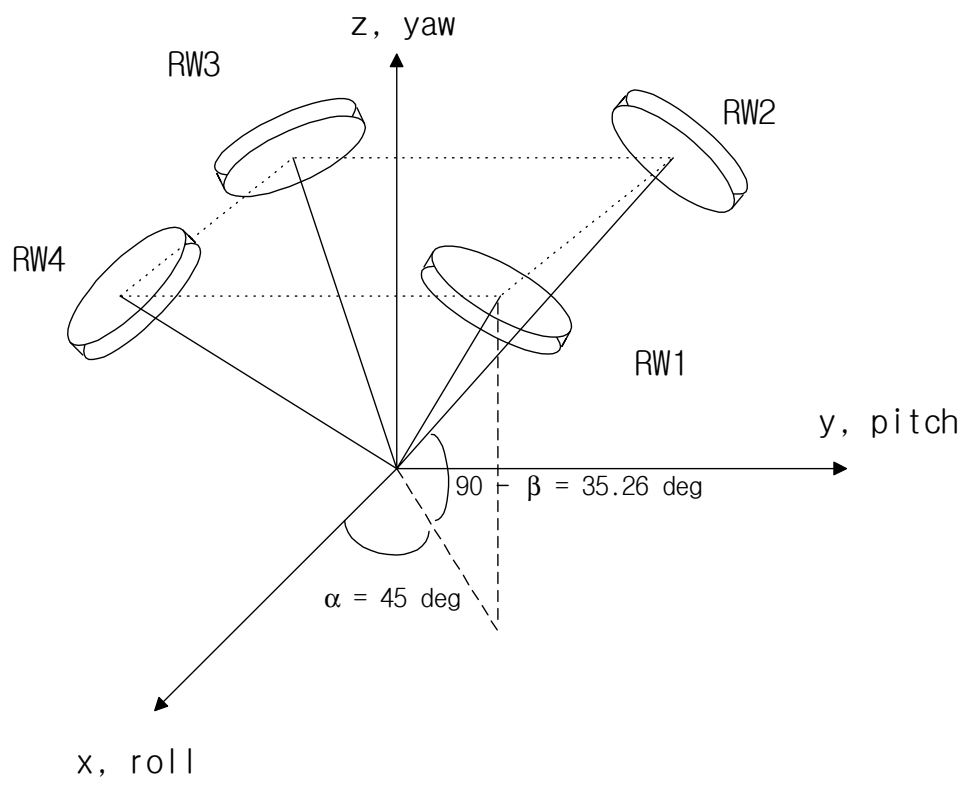


Figure 1: KOMPSAT Reaction Wheel Cluster Configuration in BFC

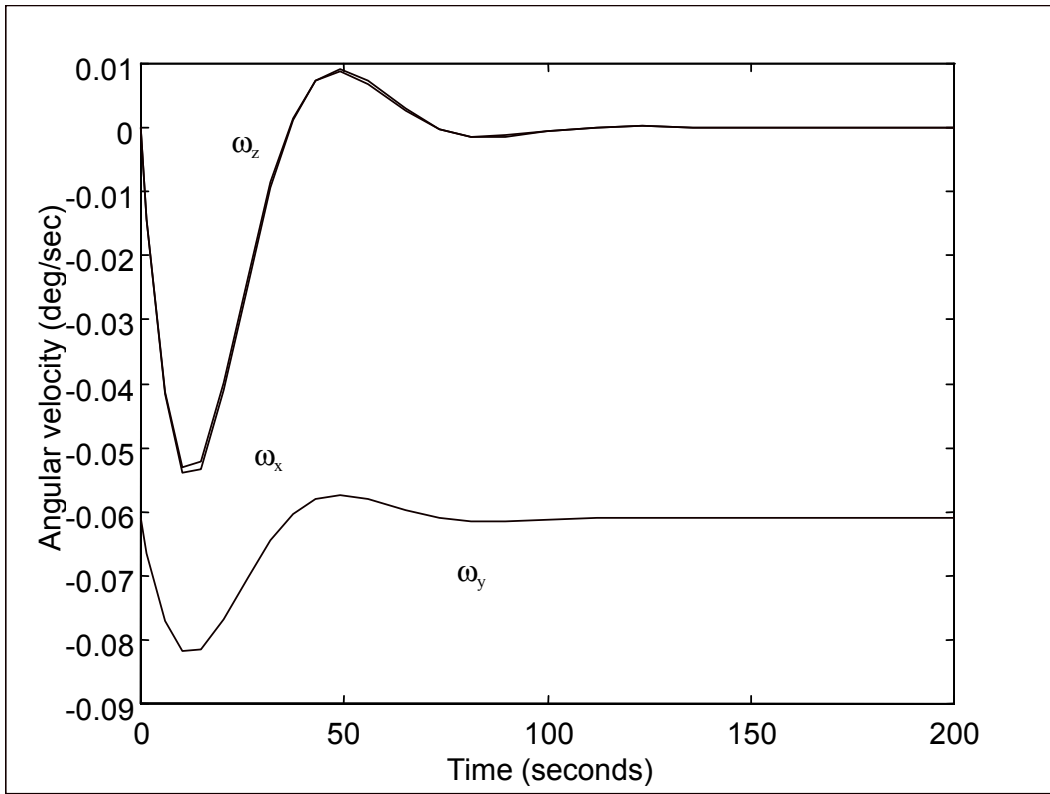


Figure 2: PD Control, Angular Velocity Versus Time

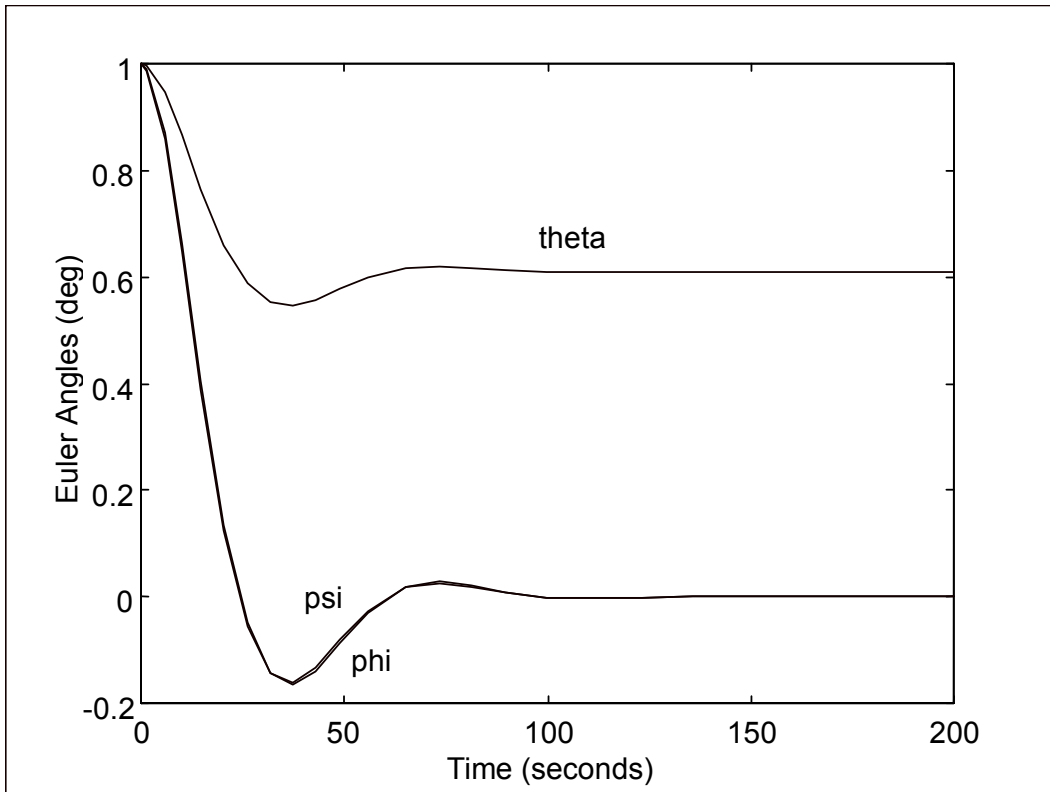


Figure 3: PD Control Euler Angles Versus Time

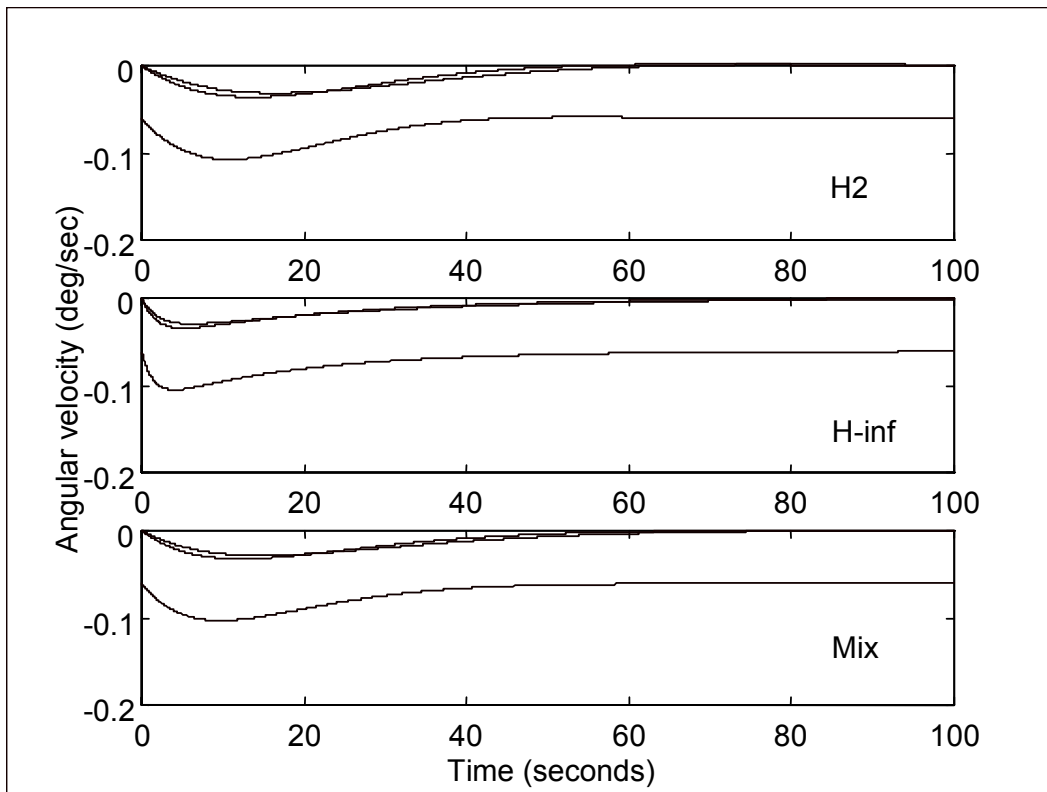


Figure 4: Angular Velocity Versus Time

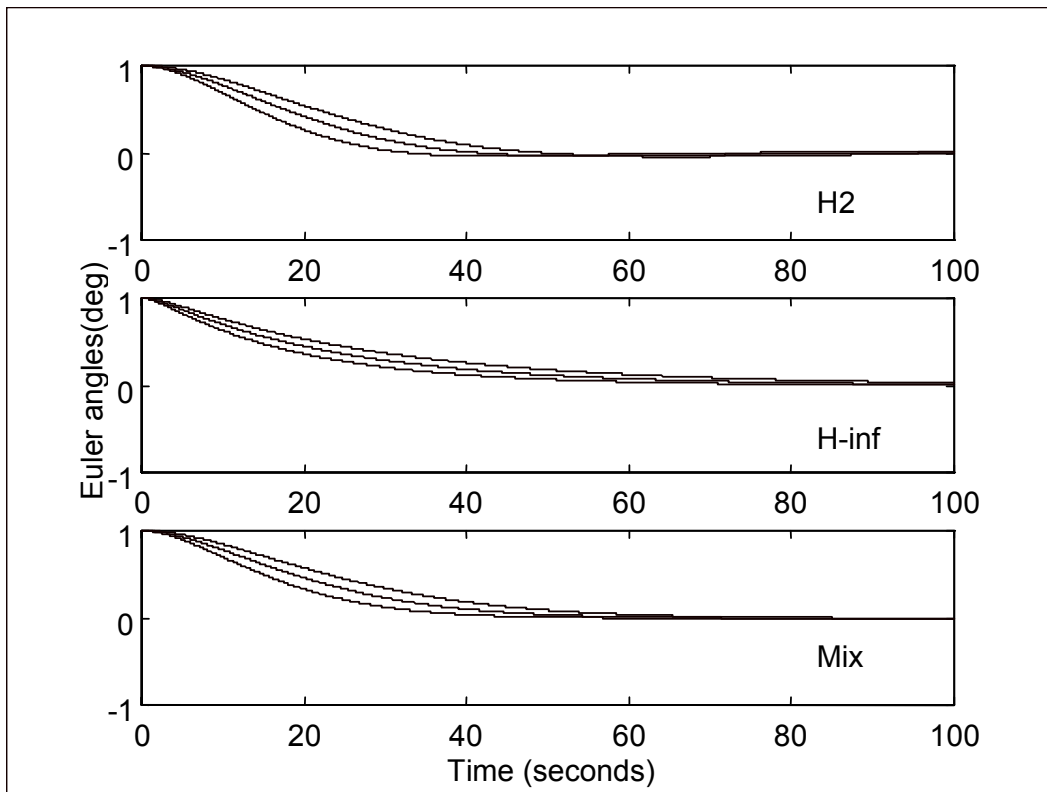


Figure 5: Euler Angles Versus Time

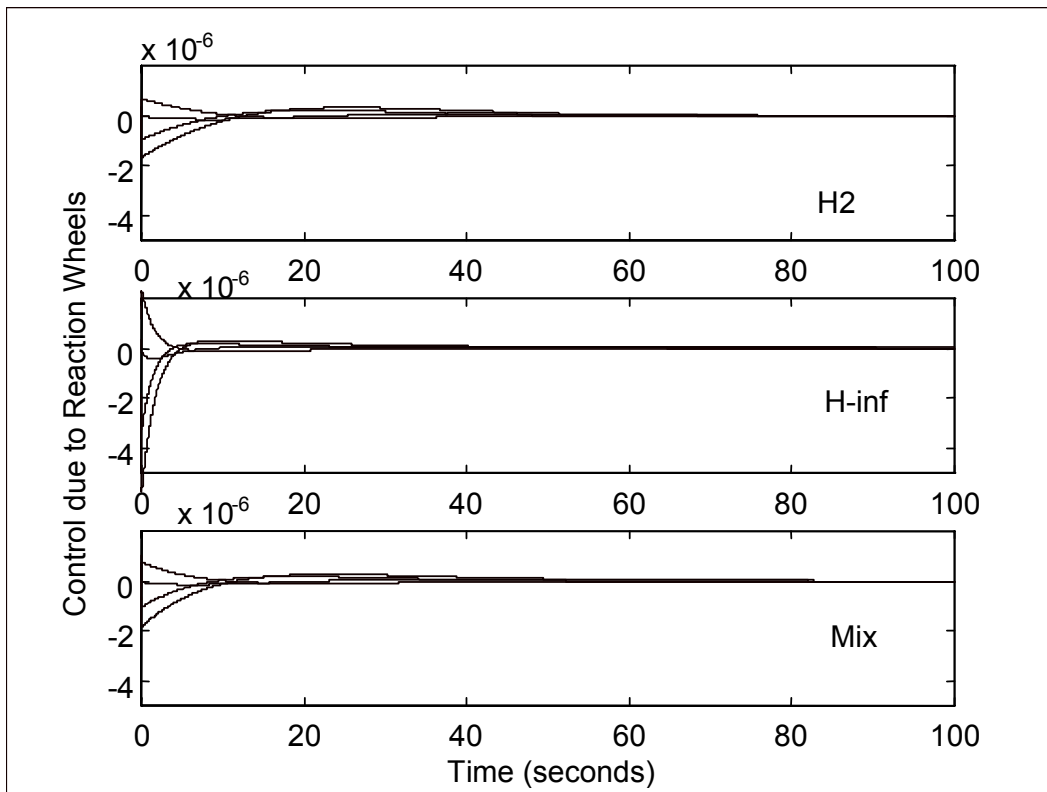


Figure 6: Control Action due to Reaction Wheels Versus Time

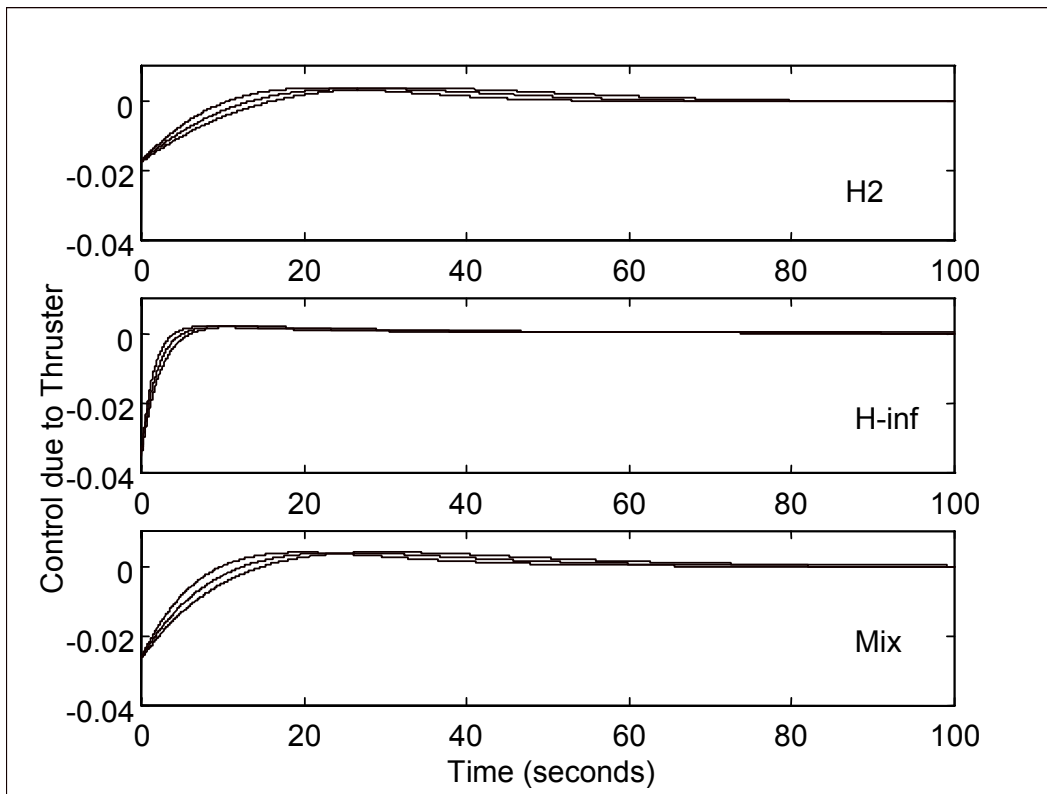


Figure 7: Control Action due to Thruster Versus Time